



PERGAMON

International Journal of Plasticity 20 (2004) 523–542

INTERNATIONAL JOURNAL OF
Plasticity

www.elsevier.com/locate/ijplas

An experimental study on grain deformation and interactions in an Al-0.5%Mg multicrystal

Nian Zhang, Wei Tong*

Department of Mechanical Engineering, 219 Becton Center, Yale University, New Haven, CT 06520-8284, USA

Abstract

Heterogeneous plastic deformation behavior of a coarse-grained Al-0.5%Mg multicrystal was investigated experimentally at the individual grain level. A flat uniaxial tensile specimen consisting of a single layer of millimeter-sized grains was deformed quasi-statically up to an axial strain of 15% at room temperature. The initial local crystallographic orientations of the grains and their evolutions after 5, 12, and 15% plastic strains were measured by electron backscattered diffraction pattern analysis in a scanning electron microscope. The local in-plane plastic strains and rigid body rotations of the grains were measured by correlation of digital optical video images of the specimen surface acquired during the tensile test. It is found that both intergranular and intragranular plastic deformation fields in the aluminum multicrystal specimen under uniaxial tension are highly heterogeneous. Single or double sets of slip-plane traces were predominantly observed on the electro-polished surfaces of the millimeter-sized grains after deformation. The active slip systems associated with these observed slip-plane traces were identified based on the grain orientation after deformation, the Schmid factor, and grain interactions in terms of the slip-plane trace morphology at grain boundaries. It is found that the aluminum multicrystal obeys neither the Sachs nor the Taylor polycrystal deformation models but deforms heterogeneously to favor easy slip transmission and accommodation among the grains.

© 2003 Elsevier Ltd. All rights reserved.

Keywords: A. Grain boundaries; A. Slip activation and transmission; A. Heterogeneous grain deformation; B. Crystal plasticity

* Corresponding author.

E-mail address: wei.tong@yale.edu (W. Tong).

1. Introduction

With the expanding knowledge on the plasticity of single crystals, the plastic deformation behavior of a polycrystalline aggregate can be analyzed numerically in great details over a wide range of length scales (Asaro, 1983; Bassini, 1994; Dawson, 2000; Schacht et al., 2003; Kaczmarek, 2003). The inclusion of material microstructure in polycrystal simulations provides highly quantitative insights on the micromechanical processes of crystal plasticity while the computational costs are increasingly affordable (Barbe et al., 2001; Goh et al., 2003; Kim and Oh, 2003; Staroselsky and Anand, 2003). Nevertheless, an accurate polycrystal plastic deformation model may not be created successfully by a simple extension of single crystal models with additional accounting of just the shapes and orientations of individual grains (Weiland and Becker, 1999). A better understanding of grain interactions and grain boundary behavior has been recognized to be the key to improve the modeling of plasticity of polycrystalline materials (Evers et al., 2001). In particular, grain boundaries in metals and alloys may have rather different defect microstructures and chemical compositions than those of the grain interiors and single crystals. The existence of grain boundaries may affect slip activation and transmission in a complex manner (Asaro, 1983; Lehockey et al., 1998). The grain interactions have also been shown to influence the initiation and growth of unstable plastic flow patterns leading to strain localization in aluminum alloys (Korbel, et al., 1986; Yang et al., 2001). Thus, there is a need to study how the slips are activated and propagated in the presence of grain boundaries and how to refine, accordingly, the existing continuum crystal plasticity models based on the experimental observations.

Many detailed finite element polycrystalline simulation analyses have been carried out to investigate grain interaction (e.g., Becker, 1991; Becker and Panchanadeeswaran, 1995; Sarma and Dawson, 1996; Mika and Dawson 1998; Barbe et al., 2001) and some enhanced hardening models in crystal plasticity have also been proposed to account for intergranular and intragranular stress and rotation heterogeneities (Miller and Dawson, 1997; Horstemeyer and McDowell, 1998; Evers et al., 2001; Tabourot et al., 2001; Raabe et al., 2002). The evaluation on the success of the finite element analyses using various crystal plasticity models against experiments has largely been done at the macroscopic level in the past, such as comparing the overall macroscopic stress-strain behavior (including the Hall–Petch relationship accounting for the effect of the average grain size on yield stress), material anisotropy or texture prediction, and shear localization. Direct comparisons between experiments and modeling on the texture evolution (lattice rotations) and deformation inhomogeneities at the individual grain level would provide a more rigorous and comprehensive assessment on crystal plasticity models.

Experimentally, local grain interactions and grain boundary behaviors can be best examined using samples made of either bicrystals and tricrystals, or two-dimensional (2D) multicrystals with single layered grains. While detailed deformation and texture measurements can also be made on the surface grains of a 3D polycrystal sample, the effects of grain deformation and interaction below the surface layer may not be easily assessed without direct measurements of local stresses of the surface grains

(Bretheau et al., 1984; Allais et al., 1994; Panchanadeeswaran et al., 1996; Becker, 1998; Pang et al., 2000; Sauzay, 2001). Bicrystal and tricrystal samples with straight boundaries have been used to investigate the slip transmission, slip heterogeneities and lattice curvature evolution (Rey and Zaoui, 1980, 1982; Clark et al., 1992; Sun et al., 2000). Difficulties in sample preparation, especially for commercial alloys, have limited the application of bicrystals and tricrystals for investigating experimentally grain interactions in a polycrystalline aggregate. Experiments on quasi-2D single layer multicrystals have gained increasing acceptance in recent years for studying the complex grain interactions in a plastically deforming polycrystalline solid (Skalli et al., 1985; Yao and Wagoner, 1993; Ziegenbein et al., 1998; Weiland and Becker, 1999; Delaire et al., 2000; Eberle et al., 2000; Mohamed et al., 1997, 2000; Tabourot et al., 2001; Raabe et al., 2001). Multicrystals with single-layered grains provide an experimentalist a variety of grain boundary interactions in terms of local stress and strain heterogeneities in a single sample and are also particularly suitable for constructing simple 3D finite element models using crystal plasticity (Havlicek et al., 1990; Weiland and Becker, 1999; Delaire et al., 2000; Raabe et al., 2001).

Experiments on 2D multicrystals have been carried out either in plane strain compression (e.g., Skalli et al., 1985; Weiland and Becker, 1999; Raabe et al., 2001) or uniaxial tension (e.g., Yao and Wagoner, 1993; Delaire et al., 2000). While plane strain compression can achieve more stable plastic flow up to large strains, the boundary conditions are more complicated due to friction and asperity contact. Furthermore, in-situ measurements of local strain distributions are difficult to carry out. Uniaxial tension tests have the advantage of simpler and more controlled boundary conditions and the availability of both local lattice orientation and plastic deformation measurements on specimen surfaces. Although the overall strain level of stable plastic deformation in a tensile test is typically limited to about 10–20% due to necking instability, such a strain range, nevertheless, covers many important applications such as fatigue, fracture, and secondary sheet metal forming. As the center part of the gage section of a flat tensile sample is much less affected from the gripping effects at the both ends, uniaxial tension stress loading is prevalent. Unlike the plane strain compression or crack-tip stress field (Shield and Kim, 1994; Weiland and Becker, 1999), such a simple stress state allows more reliable estimates of Schmid factors of each grain in a multicrystal. Indeed, when single-layered grains in a multicrystal sample are subjected to a simple loading condition such as uniaxial tension, the active slip systems during the deformation may be determined by the known crystallographic orientation via the EBSD analysis, the slip trace angles formed with respect to the tensile loading axis, and the estimated local Schmid factors (Yao and Wagoner, 1993; Delaire et al., 2000).

The aim of this paper is to report an experimental investigation on the grain-level heterogeneous plastic deformation behavior of a coarse-grained aluminum binary alloy Al-0.5%Mg multicrystal under uniaxial tension. The experimental methodology of this investigation consists of interrupted tensile tests of the aluminum multicrystal with the aid of electron backscattered diffraction (EBSD) for local texture measurements (Adams, 1993; Schwartz et al., 2000), digital image correlation (DIC)

for local in-plane surface deformation measurements (Bruck et al., 1989; Vendroux and Knauss, 1998; Tong, 1997, 1998; Smith et al., 1998; Li, 2000; Schroeter and McDowell, 2003), slip plane traces observation of polished grain surfaces (Barret, 1952; Yao and Wagoner, 1993; Wasserbäch, 1995; Delaire et al., 2000; Perocheau and Driver, 2002), and deformation kinematics analysis of crystallographic slips (Asaro, 1983; Bassini, 1994). First, the multicrystal material and experimental procedure will be described. Experimental results will then be presented in terms of both overall and local plastic deformation behaviors of the multicrystal. Active slip systems corresponding to the observed slip-plane traces on each grain surface will be determined based on the local crystallographic orientation, the Schmid factor, and the change of the morphology of the slip-plane traces across grain boundaries. The origins and nature of the heterogeneous deformation and rotation fields in the grain interiors and around grain boundaries and junctions will be discussed.

2. The experimental procedure

2.1. Sample preparation and microtexture characterization

A binary aluminum alloy Al-0.5wt%Mg was cast in a mold that was chilled only at the starting end. The cast structure was comprised of columnar grains that had grown predominantly in the casting direction with millimeter-sized grains. Most grains had the (001) orientation in the casting direction (Weiland and Becker, 1999). A flat slab of 1.1 mm in thickness was machined from the cast polycrystal with the slab surface perpendicular to the casting direction. A compact tensile specimen was then cut from the coarse-grained aluminum slab. The rectangular gage section of the specimen had a dimension of 14.5 mm×3 mm×1.1 mm and contains a few dozen single-layer millimeter-sized grains (see Fig. 1). After stress relief annealing at 250 °C for 2 h, one side of the tensile specimen was mechanically polished with 0.25 μm diamond paste and then electro-polished. Such a surface treatment was found necessary for obtaining high quality electron backscattered diffraction (EBSD) patterns in microtexture measurements and this surface is identified as the *polished surface* in this investigation. The other flat surface of the tensile specimen was decorated with fine, random black ink speckles to facilitate the grain-scale strain mapping measurements by digital image correlation and this surface is identified here as the *ink-decorated surface*. Two larger ink marks were made on the polished side of the flat sample for aligning the initial EBSD scan directions and for locating the scanned regions in subsequent EBSD measurements.

The tensile specimen was first placed inside the vacuum chamber of a Philips XL30 scanning electron microscope. The polished surface was scanned by an integrated EDAX-TSL energy dispersive analysis system (EDS) and orientation imaging microscopy system (OIM) installed on the XL30 SEM to obtain the microtexture information of the individual grains of the tensile specimen. The crystallographic orientations of grains were determined within an accuracy of 1° by

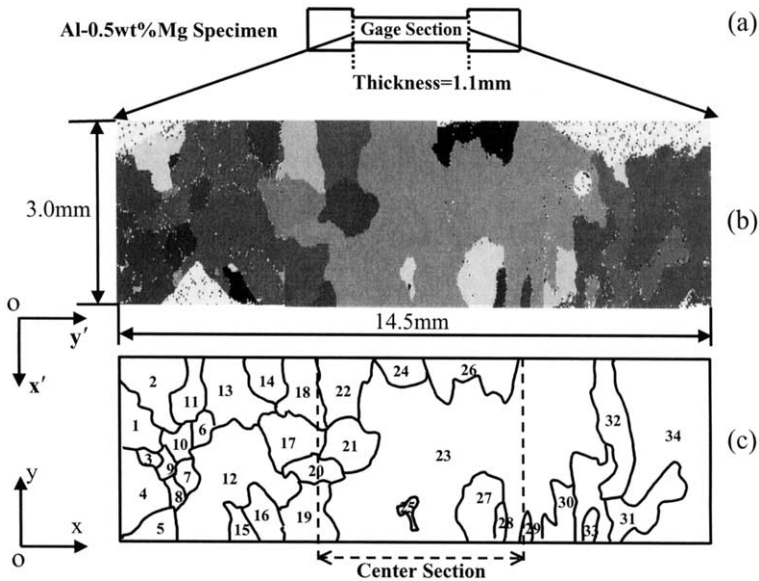


Fig. 1. The Al-0.5wt.%Mg multicrystal tensile specimen: (a) the schematic of the flat specimen; (b) the grayscale representation of the EBSD microtexture measurements; (c) the outline map of the individual grains (numbering 1–34) in the gage section of the specimen. The specimen coordinate system $x'y'z'$ used by the EBSD analysis and the specimen coordinate system xyz of the uniaxial tension test are also defined.

the EBSD analysis. Since the grain size is rather large (usually 1 mm or larger in terms of the in-plane dimension), multiple $3\text{ mm} \times 3\text{ mm}$ EBSD scans were acquired with a scanning step of $20\ \mu\text{m}$. Fig. 1 (b) shows the initial grain morphology of the gage section of the Al-0.5%Mg tensile specimen obtained from the EBSD analysis (different gray levels represent grains with different orientations). The coordinate system $x'y'z'$ is the sample coordinates defined by the EDAX-TSL orientation imaging microscopy system and the coordinate system xyz is the tensile specimen coordinate system used in the data analysis (see Section 2.3 in the following). The x -axis is the tensile loading direction, the y -axis is the transverse direction, and the z -axis is normal to the flat surface of the tensile specimen (parallel to the casting direction). Fig. 1 (c) shows the outline map of the grain boundaries that were drawn schematically in solid lines according to the EBSD analysis results and slip-plane traces observed on the deformed grains using electron microscopy. An identification number was assigned to each grain and a total of 34 grains were shown in Fig. 1 (c). Some smaller grains were omitted in the grain boundary outline map of the tensile specimen. The white regions with black dots at the top left and right corners and at the bottom-left corner in Fig. 1 (b) are places on the polished surface of the tensile specimen where high quality EBSD patterns could not be obtained. The morphology of the grains in those regions on the polished surface was nevertheless clearly revealed by optical and electron microscopy after 5, 12, and 15% plastic deformation. Fig. 2 shows an optical image of the grain morphology on the polished surface in the center section of the tensile specimen after 12% overall axial deformation.

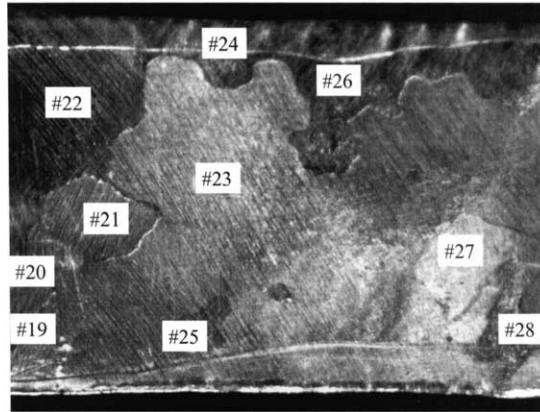


Fig. 2. Optical image of the center section of the polished surface of the aluminum multicrystal after 12% uniaxial tensile strain. A total of ten grains (19–28) are shown to be within the field of view of the image (see also Fig. 1c).

Grain boundaries were unambiguously identifiable on the electro-polished surface at proper magnifications and they were found to be completely consistent with the EBSD results (see the center section of the grain boundary outline map Fig. 1 (c)). Optical images of the ink-decorated surface were also taken at various magnifications after 12% plastic deformation. The fine ink markers (used to enhance the image contrast for strain mapping measurements by image correlation) were removed using chemical solvents. Grain boundaries on the ink-decorated surface were more difficult to locate but they were nevertheless identified at higher magnifications. The grain morphology on both surfaces of the tensile specimen after 12% axial strain was found to be nearly identical, indicating that the grain boundaries were nearly straight along its thickness direction (z -axis). Fig. 3 shows the inverse pole figures (IPF) of the center section of the specimen for the normal, axial, and transverse directions (corresponding to the z , x , y -axis respectively in Fig. 1). The inverse pole figure along the direction normal to the specimen surface shows a strong concentration of (001)-crystallographic orientations due to the directional casting and grain growth process in preparing the Al-0.5%Mg material. There exist

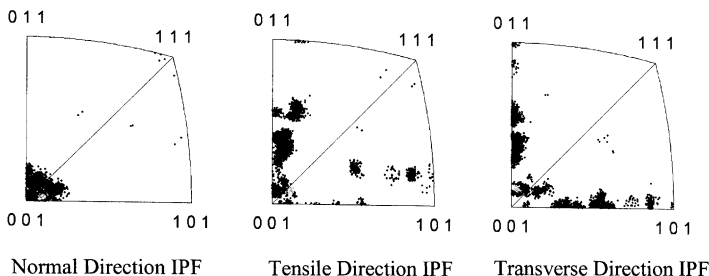


Fig. 3. Inverse pole figures of normal, axial, and transverse directions for the center section of multicrystal specimen.

nevertheless some diverse grain orientations within the plane of the flat surface of the specimen (see the inverse pole figures in the axial and transverse directions in Fig. 3). Consequently, the Al-0.5%Mg multicrystalline tensile specimen was deemed to be able to provide a range of grain boundary interactions for the current investigation.

2.2. *The testing details*

After being analyzed by the EDAX-TSL orientation imaging microscopy system installed on the Phillips XL30 SEM, the tensile specimen was then taken out of the SEM vacuum chamber and mounted on a mini-tensile test apparatus in open air. The tabletop mini-tensile test machine has a dimension of 102 mm×127 mm×50 mm, a total screw travel of 50 mm, and a maximum load capacity of 4500 N. A computer integrated stepping motor control and data/image acquisition system was used to carry out the tensile test automatically. The speed of the stepper motor was set to ten turns per minute with each turn corresponding to a total of 200 steps and an axial displacement of 6 μm. An average strain rate of 5×10^{-5} 1/s was realized during the test. The time history of axial load and overall displacement of the crosshead was recorded at a sample rate of 8 Hz during the test. The noise level in the load measurement is about ±0.1 N. The ink-decorated surface of the entire gage section of the specimen was first imaged by a digital video CCD camera under white light illumination and a set of 8-bit grayscale digital images (640×480 pixels) was recorded. The specimen was then stretched quasi-statically to a total strain of 5% in the first straining increment of the tensile test. A series of digital images of the ink-decorated surface were acquired in-situ at a rate of 1% plastic strain per image during the tensile test. The field of view of each digital image is about 4.3 mm×3.2 mm, which covers the entire the center section of the specimen with ten grains (nos. 19–28) (see Fig. 1c). At the end of the straining up to 5%, another set of digital images covering the entire gage section of the specimen was taken. The deformed specimen was then removed from the mini-tensile test stage and placed inside the SEM vacuum chamber again. A set of secondary electron images of the grains on the polished surface was acquired digitally at different magnifications and they were used to identify grain boundaries and slip-plane traces. EBSD scans were then carried out for each grain to obtain its current orientation after deformation. Because of the surface roughening caused by plastic deformation, automatic EBSD pattern acquisition and analysis was found to be difficult so only selected points with excellent quality of EBSD patterns were used for the orientation measurement of each grain after plastic deformation. The same procedure described above was repeated for another overall 7% straining of the tensile specimen (the second straining increment of the tensile test). The polished surface of the specimen after a total of 12% axial strain was decorated with fine ink markers and a series of ten digital images were acquired in-situ during the final straining increment of 3% (resulting a total of axial strain of 15% in the tensile specimen). Digital images of the original ink-decorated surface of the specimen were also acquired at the same magnification and field of view before and after the final straining increment.

2.3. Data analysis

The in-plane plastic strain distribution on the specimen surface was obtained by incrementally correlating the acquired digital images of the ink-decorated specimen surface (Tong, 1998; Li, 2000). A total of 14 digital images acquired from both the first 5% straining increment and the second 7% straining increment were analyzed and the average axial true strain were obtained over the center section of the specimen. Combining the load measured at the time when each digital image was acquired, the overall uniaxial tensile stress–strain response of the ten grains in the center section of the specimen was obtained. By assuming zero volume change due to plastic straining, the average plastic strain ratio of the 10 grains was computed from the measured average axial and transverse true strains. The in-plane strains and in-plane rigid body rotation were measured locally at points spaced 0.07 mm apart in both axial and transverse directions with a gage size of about 0.25 mm × 0.25 mm. Each deformation map consists of 54 × 44 (= 2376) grid points. Following the procedure suggested by Smith et al. (1998), an accuracy in local strains was estimated to be 0.03% or better using these image processing parameters. A similar set of correlation parameters were also used for processing the images acquired from both the ink-decorated and polished surfaces of the specimen during the final straining increment of 3%.

Based on the grain orientation measurements by the EBSD analysis at the 0, 5, 12, and 15% strain levels, the evolution of local microtexture of the multicrystalline specimen (changes of the grain orientations and grain boundary misorientations) were analyzed using the OIM software package (part of the EDAX-TSL orientation imaging microscopy system). Angles of the slip-plane trace on the polished surface of the grains were measured from the secondary electron digital images acquired by the Phillips XL30 SEM. The slip direction and slip plane normal vectors \mathbf{s} and \mathbf{m} of the 12 FCC slip systems in each grain were expressed in the tensile specimen coordinate system xyz as

$$\mathbf{s} = \mathbf{G}^{-1}\mathbf{s}_0, \quad \mathbf{m} = \mathbf{G}^{-1}\mathbf{m}_0, \quad \mathbf{G} = \mathbf{g}\mathbf{g}', \quad (1)$$

where \mathbf{s}_0 and \mathbf{m}_0 are the slip direction and slip plane normal vectors in the crystallographic coordinate system, \mathbf{g} is the orientation matrix of a grain defining the position of the crystallographic coordinate system with respect to the OIM sample coordinate system $x'y'z'$ (Schwartz et al., 2000), and \mathbf{g}' is the rotation from the tensile specimen coordinate system xyz to the OIM sample coordinate system $x'y'z'$ (see Section 2.1). Table 1 shows the Schmid and Boas notation for FCC slip systems used in the present investigation. The resolved shear stress on each slip system was computed for a given stress state in a grain via:

$$\tau = (\boldsymbol{\sigma} \cdot \mathbf{m}) \cdot \mathbf{s}, \quad (2)$$

where $\boldsymbol{\sigma}$ is the Cauchy stress tensor expressed in the tensile specimen coordinate system xyz . In this investigation, the uniaxial tension along the x -axis was assumed and the Schmid factor was computed as the resolved shear stress with a unit tension

Table 1
Schmid and Boas notation for slip systems of FCC crystals

Slip system	Slip plane	Slip direction
A2	($\bar{1}11$)	[$0\bar{1}1$]
A3	($\bar{1}11$)	[101]
A6	($\bar{1}11$)	[110]
B2	(111)	[$0\bar{1}1$]
B4	(111)	[$\bar{1}01$]
B5	(111)	[$1\bar{1}0$]
C1	($\bar{1}\bar{1}1$)	[011]
C3	($\bar{1}\bar{1}1$)	[101]
C5	($\bar{1}\bar{1}1$)	[$1\bar{1}0$]
D1	($1\bar{1}1$)	[011]
D4	($1\bar{1}1$)	[$\bar{1}01$]
D6	($1\bar{1}1$)	[110]

stress. Using the rigid viscoplastic approximation, the kinematics of crystallographic slips gives the rate of plastic deformation tensor as

$$\mathbf{D}^p = \sum_i \dot{\gamma}^i (\mathbf{s}^i \otimes \mathbf{m}^i + \mathbf{m}^i \otimes \mathbf{s}^i) / 2, \tag{3}$$

where $\dot{\gamma}^i$ is the slip rate on the i -th slip system ($\mathbf{s}^i, \mathbf{m}^i$) in the current configuration. The three in-plane components of the rate of plastic deformation tensor were computed approximately from the incremental strain mapping by image correlation. When the in-plane plastic deformation in a grain is induced predominantly by only one slip system, the slip on the highly active slip system may be estimated using Eq. (3). The rotation \mathbf{R}_G of the crystallographic lattice in a grain undergoing plastic deformation was computed according to

$$\mathbf{R}_G = \tilde{\mathbf{G}}^{-1} \mathbf{G}, \quad \mathbf{s} = \mathbf{G}^{-1} \mathbf{s}_0, \quad \tilde{\mathbf{s}} = \tilde{\mathbf{G}}^{-1} \mathbf{s}_0, \tag{4}$$

where \mathbf{G} and $\tilde{\mathbf{G}}$ are the orientation matrices of the grain before and after plastic deformation respectively. The difference between the in-plane rigid body rotation (measured by image correlation) and the in-plane component of the lattice rotation in a grain may be used to estimate the rotation due to plastic spin in the crystal.

The angle α between the slip direction and the specimen surface normal and the angle β between the x -axis and the slip plane trace of each of the four FCC slip planes in a grain were computed as

$$\alpha = \arccos(s_z), \quad \beta = \arctan(-m_x/m_y). \tag{5}$$

The potentially active slip system of each experimentally observed slip plane trace was identified based on the predicted intersection line between the slip plane and the xy -plane of the specimen (usually within 5° of less of the angle β), the value of the estimated Schmid factor τ , and the out-of-plane component of

the slip direction vector (the angle α). The grain boundaries in the tensile specimen were characterized by a misorientation \mathbf{M}_{12} between the orientations \mathbf{G}_1 and \mathbf{G}_2 of the two neighboring grains 1 and 2, namely

$$\mathbf{M}_{12} = \mathbf{G}_1^{-1} \mathbf{G}_2. \quad (6)$$

The initial misorientation angles between grain 23 and the surrounding grains in the center section of specimen are shown in Fig. 4.

3. Experimental results

3.1. The overall plastic deformation behavior of the multicrystal

The Al-0.5%Mg multicrystalline tensile specimen was stretched up to a total axial strain of 15% in three straining increments (5, 7, and 3%) in this investigation. The average uniaxial tensile true stress vs true strain curve of the multicrystal (more precisely the ten grains in the center section of the specimen) during the first two straining increments of the tensile test is shown in Fig. 5. The true strain was obtained by averaging the in-plane axial strain over a total of 2376 grid points measured by image correlation for the center section of the specimen. True stress was obtained by dividing the measured force by the current cross-section area, assuming volume constancy during plastic deformation. The volume constancy assumption was also used to compute the plastic strain ratio R (transverse strain divided by the thickness strain) and the results on R (average value is

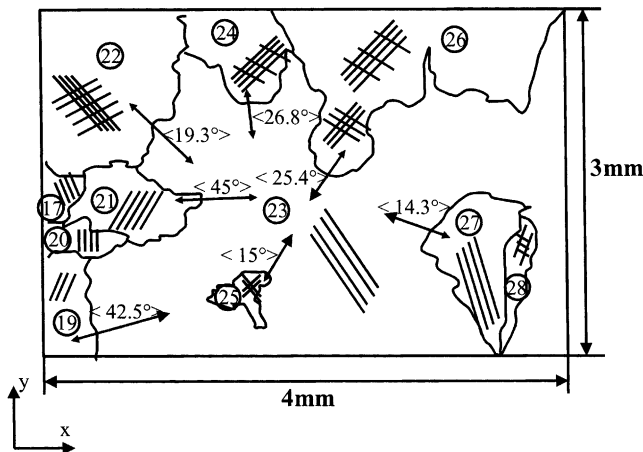


Fig. 4. A schematic view of the grains and their misorientations at the center parts of Al-0.5wt.%Mg alloy sample. The primary and secondary (if any) slip-plane traces are also shown schematically for each grain. Misorientations across grain boundaries are marked with angles (in degrees) and double-ended arrows.

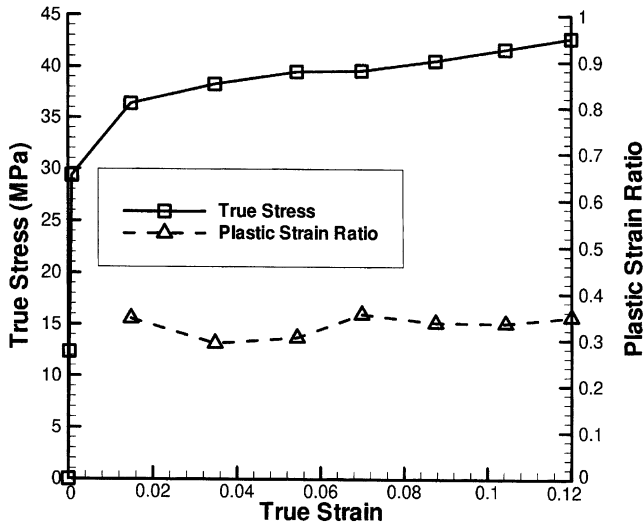


Fig. 5. Uniaxial tensile plastic stress–strain curve (solid lines) and average plastic strain ratios (dashed lines) of the multicrystal tensile specimen.

about 0.32) are also shown in Fig. 5. As the material volume used to obtain the overall response of the multicrystal contains about ten single-layer grains ($V \approx 13 \text{ mm}^3$), the overall stress–strain curve may be regarded as that of a strongly textured 2D polycrystalline material.

3.2. Local grain deformation and rotations

Detailed information about the local deformation and rigid body rotations at the grain level were obtained by digital image deformation mapping. Representative results of the local plastic deformation field (the elastic strain was assumed to be negligible) and their in-plane rigid body rotations of the ten Al-0.5%Mg grains at 12% tensile true strain are shown in Fig. 6(a) and Fig. 6(b). Fig. 6(a) is the result of the contour plot of the axial strain distribution measured on the *ink-decorated surface* overlaid on the top of the optical image of the *polished surface* of the deformed Al-0.5%Mg grains shown in Fig. 2. As shown in Fig. 6(a), the in-plane axial plastic strain is not uniform at all, especially in large grains such as grain 23. The measured in-plane rigid body rotation field at the end of the 12% plastic strain increment is shown in Fig. 6(b). There is a clear correspondence between the high strain gradient zones and high rigid body rotation gradient zones in grain 23 as expected. A diffuse macroscopic shear zone around the interior region of grain 23 is also observed to extend more or less continuously across the grain boundaries (say, between grain 22 and grain 23) and to cover the entire sample width. Fig. 6(c) shows the cumulative plastic strain along the centerline of specimen at seven selected overall axial strain levels in the axial direction during the entire tensile test. The shape of the strain distribution profiles does not change significantly over the entire 12% plastic

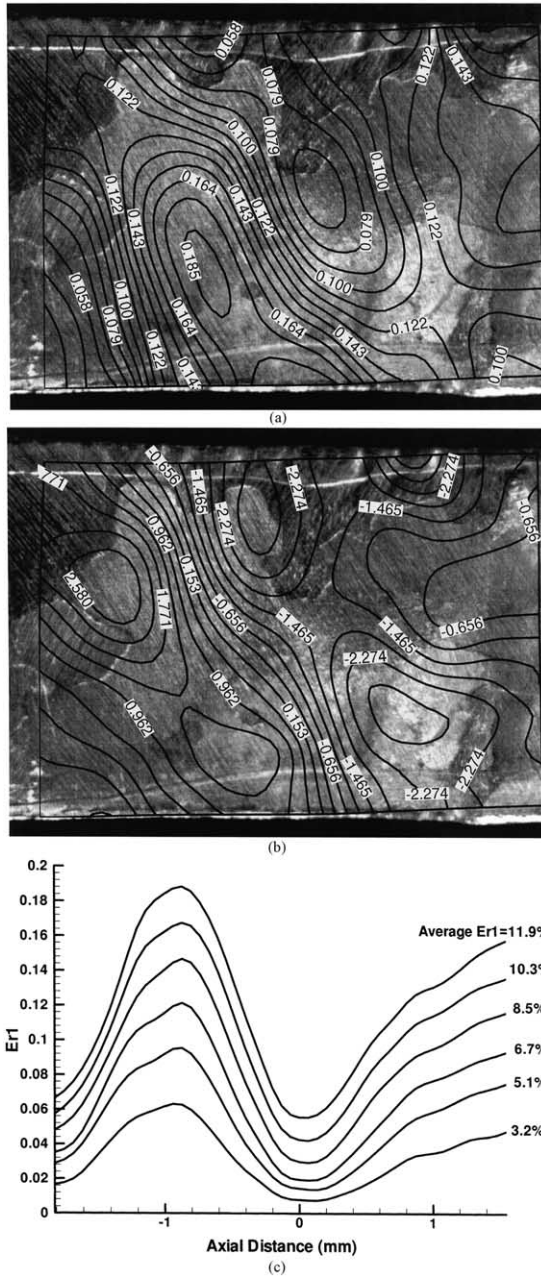


Fig. 6. Local in-plane plastic deformation measured on the ink-decorated surface of the multicrystal: (a) the cumulative axial plastic strain distribution after an overall 12% deformation; (b) the cumulative in-plane rotation angle (degrees) after an overall 12% deformation; (c) variations of the cumulative axial plastic strain along the centerline of the tensile specimen at selected overall strain levels. The field of view of the strain maps is similar to the optical image shown in Fig. 2.

deformation history and it indicates that the underlying crystallographic slips in the grains that were contributing to the plastic deformation were stable. The large grain 23 deforms highly non-uniformly under uniaxial tension (as both the peaks and valleys in Fig. 6(c) are within grain 23). Fig. 7 shows the distribution of *incremental* axial strains measured on the *polished surface* of the tensile specimen deformed from 12 to 15%. Again, the deformation concentrated mostly within the same area of the large grain 23 as shown in Fig. 6(a). The local lattice rotations of single-layer grains were found to increase with the increasing axial strain level and they were usually no more than ten degrees after 15% deformation based on the comparison of the crystallographic orientation measurements by the EBSD analysis before and after deformation [see Eq. (6) and Table 2]. At the spatial resolution $0.25\text{ mm}\times 0.25\text{ mm}$ of in-plane strain mapping measurements by image correlation, no clear discontinuity of local strains was detected around the grain boundary regions.

3.3. Activated slip systems of observed slip-plane traces in each grain

As shown in Fig. 4 schematically, only single (grains 19, 20, 21, 23, and 27) and double (grains 22, 24, 25, 26, and 28) sets of slip-plane traces were clearly observed on the initially polished surfaces of the grains in the aluminum multicrystal at 5, 12, and 15% axial strain levels. No significant change of the slip-plane trace morphology was observed except the slip-plane traces became more densely packed with the increasing axial strain levels. Using the orientations (the Euler angles) of the ten grains (19–28) and the angles of their slip-plane traces at 15% axial strain, the potentially active slip systems that might be associated with the observed slip-plane

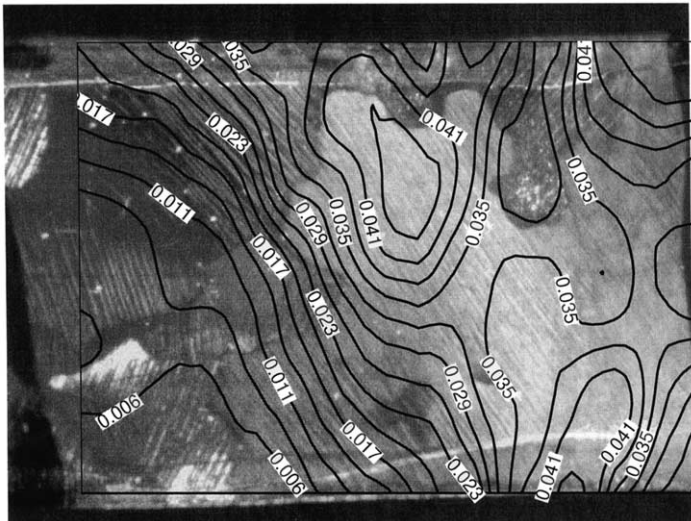


Fig. 7. The incremental in-plane axial plastic strain distribution measured on the polished-surface of the multicrystal. The multicrystal deformed approximately an average axial strain of 3% (from 12 to 15% overall axial strain).

Table 2

Summary on the crystallographic orientations and some active slip systems in the ten grains 19–28

Grain ID	Initial orientation in radian ($\varphi_1, \psi, \varphi_2$)	Final orientation in radian ($\varphi_1, \psi, \varphi_2$)	Measured slip trace angle (degree)	System(s) & orientation(s) of observed slip traces	Misorientation angle/in-plane lattice rotation (degree)
No.19	3.128, 0.120, 3.642	1.763, 0.081, 0.185	63.4°	D4 /	9.577°/6.943°
No.20	3.014, 0.138, 2.578	2.233, 0.075, 4.858	−85.8°/−81°	C3	6.921°/5.63°
No.21	2.965, 0.103, 3.756	1.99, 0.075, 6.231	63.6°	D4 /	6.307°/4.503°
No.22	1.325, 0.105, 4.904	0.768, 0.173, 0.809	−38.6° 38.4°	B4 \ D4 /	6.859°/6.825°
No.23	0.021, 0.099, 5.889	0.107, 0.233, 1.195	−55.3°	B4 \ B4 \ D4 /	9.724°/9.664°
No.24	0.300, 0.079, 6.077	0.189, 0.098, 1.352	−39.8° 39.3°	B4 \ D4 /	7.163°/7.125°
No.25	0.955, 0.093, 5.205	1.6430, 0.161, 6.27	−45.0° 50.7°	B4 \ A3 /	11.863°/13.135°
No.26	0.241, 0.093, 6.112	5.796, 0.047, 2.06	−35.7° 40.5°	B4 \ D4 /	5.353°/4.023°
No.27	5.922, 0.093, 1.311	6.095, 0.182, 1.201	−71.3°	B4 \ B4 \ A3 /	6.331°/7.588°
No.28	0.949, 0.168, 0.644	0.745, 0.211, 0.939	−32.2° 55.7°	B4 \ A3 /	6.340°/6.581°

traces were first analyzed in terms of the expected intersection line between a slip plane and the tensile specimen surface and the Schmid factors (assuming a uniaxial tension loading condition in each grain), see Eqs. (1), (2) and (5). The identified active slip systems were then examined using the grain boundary parameters defined by Eq. (7). The identified active slip systems that were responsible for producing the experimentally observed slip-plane traces on the polished surface of the ten grains are listed in Table 2. In most cases, a slip plane was identified with high confidence to be most active and thus responsible for producing the observed slip-plane traces when the angles of the predicted and observed slip-plane traces are within 1–2° and its Schmid factors are among the highest. Among a total of possible three slip directions on the active slip plane, the one with a large Schmid factor (0.4 and higher) and a large out-of-plane component of the slip direction vector was usually selected. These slip systems are shown in bold-faced letters in Table 2. The majority of the active slip systems are found to B4 and/or D4 systems (except grain 20 with the C3 system, and grains 25 and 28 with B4 and A3 systems).

3.4. Grain interaction and slip transmission at grain boundaries

A closer examination of the morphology of the slip-plane traces around the grain boundary regions using the XL-30 scanning electron microscope was carried out to assess the nature of grain interactions. The detailed slip-plane trace morphology near some selected grain boundaries of the ten grains 19–28 are shown in Fig. 8(a)–(d). At some grain boundaries (e.g., 20C3–21D4 in Fig. 8(a), 23B4–25B4 in Fig. 8(b), 23B4–27B4 in Fig. 8(c), 23B4–28B4 in Fig. 8(d)), slip-plane traces can be seen to run continuously from one grain into another grain on the specimen surface, often with

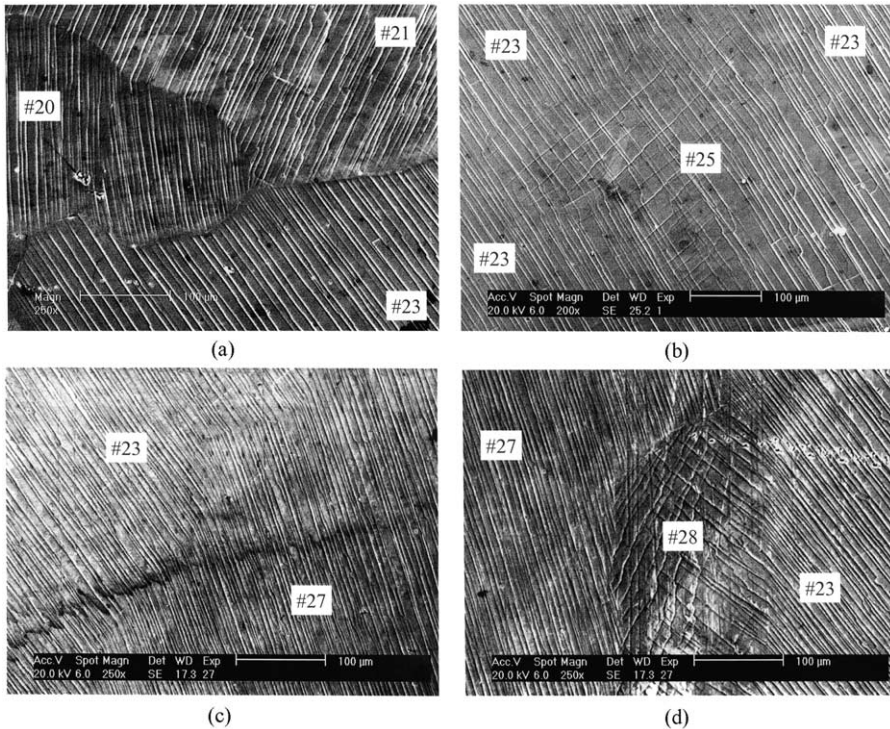


Fig. 8. The observed slip-plane trace morphology at various grain boundaries: (a) the triple junction (20, 21, and 23); (b) a single grain (25) surrounded by another grain (23); (c) the boundary between grains 23 and 27; (d) a grain (28) sandwiched between two grains (23 and 27).

only a changed orientation at the grain boundary. At other grain boundaries (e.g., 20C3–23B4 and 21D4–23B4 in Fig. 8(a), 23B4–25A3 in Fig. 8(b), and 23B4–28A3 and 27B4–28A3 in Fig. 8(d)), slip-plane traces become simply discontinuous or disappear on the specimen surface. At the triple junction among the grains 20, 21, and 23 shown in Fig. 8(a), more dense slip-plane traces were seen in grain 23 (right at the triple junction region). One can also see vaguely in Fig. 8(a) a second set of slip-plane traces (probably the slip system B4) in grain 21 near the boundary between grain 21 and grain 23.

4. Discussions

The flat, slender, and coarse-grained aluminum multicrystal under uniaxial stress loading is less constrained geometrically (especially the center part away from the two gripping ends) and the Taylor condition for polycrystals (uniform strains throughout grains) was in general not realized. The plastic deformation is highly heterogeneous from grain-level to the macroscopic level in the multicrystal. Intergranular and intragranular rotations are found closely related to the intergranular and

intragranular plastic strain heterogeneities. Furthermore, the less constrained grains favor the domination of mostly a single or two active slip systems that contributes to the increased heterogeneous lattice rotation and grain deformation fields. The presence of grain boundaries and junctions creates a rather complex stress state as dictated by the requirements of deformation compatibility and energy minimization (Clark et al., 1992; Zisman and Rybin, 1998). The local determination of the active slip systems, lattice rotations, and plastic deformation around the grain boundary regions can provide an insight into the grain interactions. Parameters such as the slip-plane intersection index M at a grain boundary and the residual Burgers vector $\delta\mathbf{b}$ have been used in the literature for characterizing the grain boundary interactions when single slip systems are dominant in both grains during plastic deformation

$$M = \mathbf{L}_1 \cdot \mathbf{L}_2, \quad \delta\mathbf{b} = \mathbf{b}_1 - \mathbf{b}_2, \quad (7)$$

where \mathbf{L}_1 and \mathbf{L}_2 are the unit vectors of two lines intersected by the slip planes of the active slip systems with the grain boundary plane at both sides, and \mathbf{b}_1 and \mathbf{b}_2 are the Burgers vectors of the active slip systems in each grain (it has been known that the slip transmission occurs at the grain boundary with a large M value and a small $|\delta\mathbf{b}|$ value, see, Clark et al., 1992). When the information on the Burgers vectors on the two active slip systems on either side of a grain boundary is unavailable, the difference between their slip direction vectors $|\delta\mathbf{s}| = |\mathbf{s}_1 - \mathbf{s}_2|$ may be used as an approximation (noting that $\mathbf{s}_1 \cdot \mathbf{b}_1 = 0$ and $\mathbf{s}_2 \cdot \mathbf{b}_2 = 0$ for edge dislocations). The actual active slip systems of the observed slip-plane traces in the grains were consequently checked based on the parameters M and $|\delta\mathbf{s}|$ between neighboring grains. The grain boundaries that have apparent “continuous” crossing slip-plane traces are found to have a large slip-plane intersection index M (between 0.5 and 1) and a small difference between the slip direction vectors of the two active slip systems at the grain boundary ($|\delta\mathbf{s}| < 1$). Grain interactions in the aluminum multicrystal studied here seem to promote the deformation modes (slip systems) in each grain that favor easy slip transmission and accommodation at these grain boundaries. On the other hand, the grain boundaries that have apparent “discontinuous” or disappearing slip-plane traces are found to have a relatively smaller slip-plane intersection index M (< 0.5).

The five grains 19, 20, 21, 23, and 27 appear to deform plastically up to 15% uniaxial tensile strain with a persistent pattern of a single set of slip-plane traces. Although one cannot rule out in general the possibility that there may be some very active slip systems in these grains with their slip planes being parallel or nearly parallel with the tensile specimen surface (so no slip-plane traces will be visible on the tensile specimen surface), the analyses of these five grains (assuming a uniaxial tension stress state) indicate that there is no such slip system with a Schmid factor of 0.4 or larger. It appears that the grain boundary interactions were accommodated in these grains by highly heterogeneous intergranular deformation. The in-plane plastic strain mapping results [see Figs. 6(a) and 7] strongly suggest this was indeed the case for the large grain 23 (which exhibits only a single set of slip plane traces throughout its grain interior and grain boundary regions). For smaller grains such as grain 20 shown in Fig. 8(a), the slip traces near the triple junction and away from the triple

junction have the angles of -85.8° and -81.0° respectively. The local EBSD analysis of the grain 20 indicated that there is also a noticeable change of crystallographic orientations in these two regions. In fact, the same slip system was identified to be active in both regions of the grain 20 even though the angles of slip traces are apparently different. In other words, small grains deform heterogeneously to accommodate the grain interactions by creating intragranular orientation heterogeneities. On the other hand, the five grains 22, 24, 25, 26 and 28 deform plastically under uniaxial tension by multiple slips. The two sets of the slip traces clearly observed on the polished surfaces of all of these five grains indicate that at least two slip systems with different slip planes were activated. These five grains usually have six to eight slip systems with comparably large Schmid factors (as a comparison: the five grains 19, 20, 21, 23, and 27 usually have two to three slip systems with dominantly large Schmid factors). For example, the Schmid factors of the 12 slip systems in grain 26 are 0.4245, 0.4245, 0.4075, 0.4074, 0.4062, 0.4062, 0.3906, 0.3906, 0.0183, 0.0170, 0.0169, 0.0156 and the values of the Schmid factors of the 12 slip systems in grain 27 are 0.4866, 0.4106, 0.3376, 0.2700, 0.2167, 0.1940, 0.1490, 0.1304, 0.1396, 0.0730, 0.0544, 0.0186. Grain 26 has a total of eight slip systems, with Schmid factors around 0.4, while grain 27 has only two slip systems with Schmid factors higher than 0.4.

The use of a 2D multicrystal tensile specimen with single layered grains can simplify both the theoretical analysis and finite element simulation of grain deformation and interactions to a considerable degree by assuming that the material microtexture and plastic deformation properties are the same along the thickness direction of the multicrystal tensile specimen. Because all of the experimental measurements (in-plane plastic deformation and rotation by image correlation, local crystallographic orientations and slip-plane traces of grains) were made only on the surfaces of the flat tensile specimen, one needs to examine the validity of applying such measurements to the interior part of the grains between the specimen surfaces. Experimentally, one may monitor the quality of the 2D approximation by carrying out the measurements on both surfaces of a multicrystal tensile specimen. In this investigation, the grain boundary morphology at 12% overall axial strain and the local in-plane plastic deformation increments from 12 to 15% overall axial strain were examined at the corresponding locations on both surfaces of the flat Al-0.5% multicrystal tensile specimen. The results show that the grain structures on both the ink-decorated and the polished surfaces of the tensile specimen are nearly identical as shown in Fig. 2 and the plastic strain distribution has the same spatial heterogeneity as shown in Fig. 7. It is concluded that the Al-0.5%Mg tensile specimen may well be approximated as a 2D multicrystal in the analysis.

As the aluminum multicrystal obeys neither the Sachs (uniform stress) nor the Taylor (uniform strain) polycrystal deformation models, the analysis and discussions given here can only be regarded as the first approximation with the aim to provide a *qualitative* view of the grain deformation and interactions in the multicrystal under uniaxial tension. Nevertheless, present experimental investigations provide the supporting evidence that the number of slip systems that have significant amounts of slips locally in multicrystal is usually less than five (Yao and Wagoner, 1993; Ziegenbein et al., 1998; Delaire et al., 2000; Eberle et al., 2000; Mohamed et

al., 1997, 2000; Tabourot et al., 2001). Finite element simulations of plastic deformation of single-layer multicrystal tensile samples reported by Delaire et al. (2000) indicate that most often only up to two slip systems are predominantly active in each grain at small to moderate tensile strains. Because of the continuous lattice rotation during the course of the plastic deformation (see Table 2) and the highly heterogeneous nature of grain deformation and interactions, a nonlinear finite element analysis of the tensile test using crystal plasticity model is currently underway to evaluate more quantitatively the crystallographic slips in each of the grains in the Al-0.5%Mg multicrystal. The results on the local stress fields and accumulated slips on active slip systems locally in each grain will be reported in a subsequent paper in the future.

5. Conclusions

The heterogeneous plastic deformation behavior of a coarse-grained binary aluminum multicrystal under uniaxial tension was successfully investigated at the individual grain level. By combining the high-quality local lattice orientation, slip plane trace observations, and the simple analysis of uniaxial loading (computations of Schmid factors) and grain boundary interactions, the most likely active slip system(s) of the observed slip-plane traces have been identified. The extensive experimental data (local grain orientations and their changes, local deformation gradient tensor, and slip plane trace morphology) on the local grain deformation and interactions of the multicrystal should provide an excellent basis for evaluating the crystal plasticity models by direct comparison between the experimental data and the results of a 3D finite element crystal plasticity simulation of the multicrystal.

Acknowledgements

The authors would like to thank Dr H. Weiland of Alcoa for providing the quasi-2D multicrystalline material used in this investigation and for insightful discussions. The research was primarily supported by the NSF CAREER Award to WT (Grant No. CMS-9733797). Additional supports were provided by the Alcoa Technical Center (Pittsburgh, PA), the Lawrence Livermore National Labs (Livermore, CA) and the Olin Metals Research Labs (New Haven, CT). The scanning electron microscopy facility including the EBSD attachments used in this research at Yale University was made possible in part through the NSF Grants No.CMS-9700327 and No.CTS-981338.

References

- Adams, B.L., 1993. Orientation imaging microscopy: application to the measurement of grain boundary structure. *Mat. Sci. Eng.* A166, 59–66.

- Allais, L., Bornert, M., Bretheau, T., Caldemaison, D., 1994. Experimental characterization of the local strain field in a heterogenous elastoplastic material. *Acta Metal. Mater.* 42 (11), 3865–3880.
- Asaro, R.J., 1983. Micromechanics of crystals and polycrystals. *Adv. Appl. Mech.* 23, 1.
- Barbe, F., Decker, L., Jeulin, D., Cailletaud, G., 2001. Intergranular and intragranular behavior of polycrystalline aggregates. Part I: F.E. model. Part II. Results. *Int. J. Plasticity* 17 (4), 513–563.
- Barret, C.S., 1952. *Structure of Metals*. McGraw-Hill Book Co., New York.
- Bassini, J.L., 1994. Plastic flow of crystals. *Adv. Appl. Mech.* 30, 192–258.
- Becker, R., 1991. Analysis of texture evolution in channel die compression—I. Effects of grain interaction. *Acta Metall. Mater.* 39 (6), 1211–1230.
- Becker, R., 1998. Effects of strain localization on surface roughening during sheet forming. *Acta Mater.* 46, 1385.
- Becker, R., Panchanadeeswaran, S., 1995. Effects of grain interactions on deformation and local texture in polycrystals. *Acta Metall. Mater.* 43 (7), 2701–2719.
- Bretheau, T., Mussot, P., Rey, C., 1984. Microscale plastic inhomogeneities and macroscopic behavior of single and multiphase materials. *ASME J. Eng. Mater. Tech.* 106, 304–310.
- Bruck, H.A., McNeill, S.R., Sutton, M.A., Peters, W.H., 1989. Digital image correlation using Newton–Raphson method of partial differential corrections. *Exp. Mech.* 29, 261–267.
- Clark, W.A.T., Wagoner, R.H., Shen, Z.Y., 1992. On the criteria for slip transmission across interfaces in polycrystals. *Scripta Metal. Mater.* 26, 203–206.
- Dawson, P.R., 2000. Computational crystal plasticity. *Int. J. Solids Struct.* 37 (1), 115–130.
- Delaire, F., Raphanel, J.L., Rey, C., 2000. Plastic heterogeneities of a copper multicrystal deformed in uniaxial tension: experimental study and finite element simulations. *Acta Mater.* 48 (5), 1075–1087.
- Eberle, F., Wroblewski, T., Cailletaud, G., Lebrun, J.L., 2000. Experimental and numerical approach of inter- and transgranular stress- and rotation heterogeneities in the plastic behaviour of a multicrystal. *Mater. Sci. Forum* 347, 60–65.
- Evers, L.P., Parks, D.M., Brekelmans, W.A.M., Geers, M.G.D., 2001. Enhanced modeling of hardening in crystal plasticity for FCC metals. *J. De Physique. IV : JP.* 11 (5), Pr5179–Pr5186.
- Goh, C.-H., Neu, R.W., McDowell, D.L., 2003. Crystallographic plasticity in fretting of Ti-6AL-4V. *Int. J. Plasticity* (in press).
- Havlicek, F., Kratochvil, J., Tokuda, M., Lev, V., 1990. Finite element model of plastically deformed multicrystal. *Int. J. Plasticity* 6 (3), 281–291.
- Horstemeyer, M.F., McDowell, D.L., 1998. Modeling effects of dislocation substructure in polycrystal elastoviscoplasticity. *Mech. Mater.* 27 (3), 145–163.
- Kaczmarek, J., 2003. A nanoscale model of crystal plasticity. *Int. J. Plasticity* (in press).
- Kim, H.-K., Oh, S.-I., 2003. Finite element analysis of grain-by-grain deformation by crystal plasticity with couple stress. *Int. J. Plasticity* 19 (8), 1245–1270.
- Korbel, A., Embury, J.D., Hatherly, M., Martin, P.L., Erbsloh, H.W., 1986. Microstructural aspects of strain localization in Al-Mg alloys. *Acta Metal* 34 (10), 1999–2009.
- Lehockey, E.M., Palumbo, G., Aust, K.T., Erb, U., Lin, P., 1998. On the role of intercrystalline defects in polycrystal plasticity. *Scripta Mater.* 39 (3), 341–346.
- Li, X., 2000. *Spatial Characterization of Unstable Plastic Flows in Two Aluminum Alloys*. Ph.D. Thesis., Department of Mechanical Engineering, Yale University, New Haven, CT.
- Mika, D.P., Dawson, P.R., 1998. Effects of grain interaction on deformation in polycrystals. *Mater. Sci. Eng. A: Struct. Mater.: Properties, Microstructure & Processing* 109 (1), 62–76.
- Miller, M., Dawson, P., 1997. Influence of slip system hardening assumptions on modeling stress dependence of work hardening. *J. Mechan. Phys. Solids* 45 (11-12), 1781–1804.
- Mohamed, G., Bacroix, B., Ungar, T., Raphanel, J.L., Chauveau, T., 1997. Experimental and numerical determination of the intragranular work hardening in a cold rolled multicrystal. *Mater. Sci. Eng. A: Struct. Mater.: Properties, Microstructure & Processing* 940–943.
- Mohamed, G., Bacroix, B., Lebrun, J.-L., 2000. Anisotropy of dislocation distribution and long-range internal stresses. *Mater. Sci. Forum* 347, 285–290.
- Panchanadeeswaran, S., Doherty, R.D., Becker, R., 1996. Direct observation of orientation change by channel die compression of polycrystalline aluminum—use of a split sample. *Acta. Mater.* 44 (3), 1233–1262.

- Pang, J.W.L., Holden, T.M., Wright, J.S., Mason, T.E., 2000. The generation of intergranular strains in 309H stainless steel under uniaxial loading. *Acta Mater.* 48, 1131–1140.
- Perocheau, F., Driver, J.H., 2002. Slip system rheology of Al-1% Mn crystals deformed by hot plane strain compression. *Int. J. Plasticity* 18, 185–202.
- Raabe, D., Sachtleber, M., Zhao, Z., Roters, F., Zaefferer, S., 2001. Micromechanical and macro-mechanical effects in grain scale polycrystal plasticity experimentation and simulation. *Acta Mater.* 49 (17), 3433–3441.
- Raabe, D., Zhao, Z., Park, S.-J., Roters, F., 2002. Theory of orientation gradients in plastically strained crystals. *Acta Mater.* 50 (2), 421–440.
- Rey, C., Zaoui, A., 1980. Slip heterogeneities in deformed aluminum bicrystals. *Acta Metall.* 28, 687–697.
- Rey, C., Zaoui, A., 1982. Grain boundary effects in deformed bicrystals. *Acta Metall.* 30, 523–535.
- Sarma, G.B., Dawson, P.R., 1996. Effects of interactions among crystals on the inhomogeneous deformations of polycrystals. *Acta Mat.* 44 (5), 1937–1953.
- Sauzay, M., 2001. Large plastic strains in surface grains. *J. De Physique. IV : JP.* 11 (5), Pr5309–Pr5315.
- Schacht, T., Untermann, N., Steck, E., 2003. The influence of crystallographic orientation on the deformation behaviour of single crystals containing microvoids. *Int. J. Plasticity* (in press).
- Schroeter, B.M., McDowell, D.L., 2003. Measurement of deformation fields in polycrystalline OFHC copper. *Int. J. Plasticity* 19 (9), 1355–1376.
- Schwartz, A.J., Kumar, M., Adams, B.L., 2000. *Electron Backscatter Diffraction in Material Science*. Kluwer Academic/Plenum Publishers, New York.
- Shield, T.W., Kim, K.S., 1994. Experimental measurement of the near-tip strain field in an iron silicon single-crystal. *J. Mech. Phys. Solids* 42, 845–873.
- Skalli, A., Fortunier, R., Fillit, R., Driver, J.H., 1985. Crystal rotations during the rolling of large-grained aluminum sheet. *Acta Metal* 33 (6), 997–1007.
- Smith, B.W., Li, X., Tong, W., 1998. Error assessment for strain mapping by digital image correlation. *Exp. Tech.* 22 (4), 19–21.
- Staroselsky, A., Anand, L., 2003. A constitutive model for hcp materials deforming by slip and twinning: application to magnesium alloy AZ31B. *Int. J. Plasticity* (in press).
- Sun, S., Adams, B.L., King, W.E., 2000. Observations of lattice curvature near the interface of a deformed aluminum bicrystals. *Phil. Mag.* A80, 9–25.
- Tabourot, L., Dumoulin, S., Baland, P., 2001. An attempt for a unified description from dislocation dynamics to metallic plastic behaviour. *Journal De Physique. IV.* 11 (5), Pr5111–Pr5118.
- Tong, W., 1997. Detection of plastic deformation patterns in a binary aluminum alloy. *Exp. Mech.* 37 (4), 452–459.
- Tong, W., 1998. Strain characterization of propagative deformation bands. *J. Mech. Phys. Solids* 46 (10), 2087–2102.
- Vendroux, G., Knauss, W.G., 1998. Submicron deformation field measurements, Part 2. Improved digital image correlation. *Exp. Mech.* 38 (2), 86–91.
- Wasserbäch, W., 1995. Development of the dislocation arrangement in high-purity Nb-34at% Ta alloy single crystals deformed in tension. *Phys. Stat. Sol. (a)* 151, 61–82.
- Weiland, H., Becker, R., 1999. Mesoscale deformation structures in aluminum. *Proc. of 20th Risø Int. Symposium on Mat. Sci.: Deformation-Induced Microstructures: Analysis and Relation to Properties* (J.B.Bilde-Sørensen, et al. eds.), Risø National Laboratory, Roskilde, Demark, 213–225.
- Yang, S.-Y., Li, X., Tong, W., 2001. Coarse slip bands in a single-crystalline aluminum alloy. *Materials Research Society Symposium - Proc.* v 653, Z4.9.1–Z4.9.6.
- Yao, Z., Wagoner, R.H., 1993. Active slip in aluminum multicrystals. *Acta Metall. Mater.* 41 (2), 451–468.
- Ziegenbein, A., Neuhäuser, H., Thesing, J., Ritter, R., Wittich, H., Steck, E., Levermann, M., Woltd, E., 1998. Local plasticity of Cu-Al polycrystals—measurements and FEM-simulation. *J. Phys.* IV 8, Pr8–407-Pr8-412.
- Zisman, A.A., Rybin, V.V., 1998. Mesoscopic stress field arising from the grain interaction in plastically deformed polycrystals. *Acta Mater.* 46 (2), 457–464.